Bull. Chem. Soc. Ethiop. **2024**, 38(6), 1843-1860.
DOI: https://dx.doi.org/10.4314/bcse.v38i6.26

ISSN 1011-3924
Printed in Ethiopia
Online ISSN 1726-801X

ANTIBACTERIAL ACTIVITY OF SECONDARY METABOLITES FROM THE ROOTS OF *SOLANUM DASYPHYLLUM*: A COMBINED *IN VITRO* AND IN SILICO STUDY

Dereilo Bekere Belitibo[1,2], Asfaw Meressa[1], Abiy Abebe[1], Sileshi Degu[1], Milkyas Endale[1], Frehiwot Teka Assamo[1], Tamrat Tesfaye Ayele[2], Getahun Tadesse Gurmessa[2], Fekadu Gurmessa[3], Messay Wolde-Mariam[4] and Negera Abdissa[1,2*]

[1]Traditional and Modern Medicine Research and Development Directorate, Armauer Hansen Research Institute, P. O. Box 1005, Addis Ababa, Ethiopia
[2]Department of Chemistry, College of Natural and Computational Sciences, Wollega University, Nekemte, Ethiopia
[3]Department of Biology, College of Natural and Computational Sciences, Wollega University, Nekemte, Ethiopia
[4]Pharmaceutical Manufacturing Industry and Development Directorate Sector, Armauer Hansen Research Institute, P. O. Box 1005, Addis Ababa, Ethiopia

(Received May 19, 2024; Revised September 6, 2024; Accepted September 10, 2024)

ABSTRACT. *Solanum dasyphyllum* is widely utilized for folk medicine in Ethiopia. The chromatographic separation of root extract of *S. dasyphyllum* led to the isolation of six compounds: tremulacin (**1**), scopoletin (**2**), stigmasterol (**3**), β-sitosterol (**4**), palmitic acid (**5**) and 2,3-dihydroxypropyl-9Z,12Z-octadecadienoate (**6**). The structures of the compounds were determined using NMR (1D and 2D), MS and comparison with literature data. The extract and isolated compounds were *in vitro* assayed against six bacterial strains and displaying activity against the tested strains. The extract exhibited stronger activity against *E. coli*, *K. pneumoniae*, and *P. aeruginosa*, with MIC values of 0.195±0.0, 0.391±0.0, and 0.195±0.0 mg/mL, respectively. The isolated compounds also showed good antibacterial activity with the highest activity was recorded for compound **2**, with MIC values of 0.313±0.0 mg/mL against *K. pneumoniae*, while for the ciprofloxacin is 0.195±0.0 mg/mL against the same strain. *In silico* molecular docking analyses were performed for compounds **1, 2** and **3** against *E. coli* DNA gyrase B, *P. aeruginosa* LasR protein, and *K. pneumoniae* using AutoDock Vina and showed better binding activity. The *in vitro* antibacterial results and *in silico* analysis of the compounds revealed the potential of these compounds to be lead compound for antibacterial drug discovery.

KEY WORDS: *Solanum dasyphyllum*, Chromatographic separation, Antibacterial activity, Molecular docking

INTRODUCTION

The genus, *Solanum* L. (family, Solanaceae) is one of the largest genera of the family, comprising of about 2000 species distributed in the tropical, subtropical, and temperate regions [1]. It has received considerable attention due to its economic significance and ethno-medicinal uses [1, 2]. Solanum species are rich in producing secondary metabolites including phenols, alkaloids, saponins, terpenes, flavonoids, coumarins, and carotenoids [1, 3]. Some of them have been reported to show anticancer, antioxidant, antihypertensive, anti-inflammatory, hepatoprotective, anti-obesogenic, and antidiabetic properties [1, 3-5].

Solanum dasyphyllum (*S. dasyphyllum*) is one of the species growing in Ethiopia and has been widely utilized by traditional healers for the treatment of a number of human illnesses [6-11]. The root of *S. dasyphyllum* is used to treat poisons of venomous stings and bites [8] and abdominal colic [7]. Leaves are utilized for treatment of gastrointestinal diseases, gout, and inflammation [9]. Fruits are used to treat external parasites [10]. The leaf-sap and flowers are used to treat

*Corresponding authors. E-mail: negeraabdisa@gmail.com

subcutaneous parasitic infection and as antidotes in *Strophanthus* poisoning [11]. The crude extract of the plant has been reported to exhibit pharmacological studies of antioxidant, antimicrobial, anti-inflammatory, neuromodulator, neurotoxic, and anti-venom activities [8, 12-15]. However, there is no report on the antimicrobial properties of isolated compounds from this plant. Even though the plant possesses a wide range of therapeutic values, prior scientific investigations done on this plant are not exhaustive. Thus, herein, we report the isolations and characterization of chemical constituents and evaluation of their *in vitro* antibacterial activity along with *in silico* molecular docking and absorption, distribution, metabolism, excretion, and toxicity (ADMET) analysis.

EXPERIMENTAL

General experimental procedures

All solvents and reagents used for extraction and purification were of analytical and high-performance liquid chromatography (HPLC) grade. Thin layer chromatography (TLC) analysis was performed using analytical TLC pre-coated sheets, ALUGRAM® Xtra SIL G/UV_{254} (layer: 0.20 mm silica gel 60 with fluorescent indicator $UVF_{254/365}$). Silica gel with a mesh size of 60–120 was used for column chromatography. Chromatograms were visualized on TLC by dissolving 1 g of vanillin added with 2 mL of sulfuric acid in 100 mL of 95% ethanol. After spraying, the TLC plate was heated at 110 °C for about 5 min. NMR spectra were recorded on an Avance 500 MHz spectrometer (Bruker, Billerica, MA, USA). Melting points were determined on a Japson Melting Point Apparatus (JA90161, India). For the antimicrobial analysis, Tween, pre-labeled 96-well microplate, Biosafety Cabinet (Telstar), UV-Visible Spectrophotometer (Thermo Scientific Evolution 60S), Incubator (Memmert Germany), Whirl mixer (borfax), and Mueller Hinton Broth (MHB) (Sigma-Aldrich) were used. Ciprofloxacin (Germany-Twinbrook PKWY) was used as a reference standard.

Plant materials

The root of *S. dasyphyllum* was collected from East Badewacho Worada, Hadiya Zone, in December, 2021. The plant material was identified by botanist (Prof. Sileshi Nemomisa) and the voucher specimen (No DB-01) has been deposited in Addis Ababa University Herbarium.

Extraction and isolation

The powdered roots of *S. dasyphyllum* (1 kg) were defatted first with n-hexane (5 L, 24 h) three times with shaking using mechanical shaker at a speed of 150 rpm at room temperature. The extract was filtered using Whatman No.1 filter paper. The marc was dried and extracted with methanol (5 L, 24 h) using the same procedure as above. The extracts were dried using rotary evaporator (Buchi, R-300 Switzerland) at temperatures of 40 °C to produce 8 g (0.8%) and 54 g (5.4%) of *n*-hexane and methanol extracts, respectively.

About 40 g of the methanol extract was subjected to silica gel (250 g) column chromatography, and the column was eluted with increasing polarity of EtOAc in *n*-hexane to afford 179 fractions, 40 mL each. Fractions 36–45 (eluted using n-hexane/EtOAc (9:1) were combined based on their TLC profile and further purified using preparative thin layer chromatographic with n-hexane/EtOAc (9:1) as the eluent to give compound **2** (18 mg) and compound **4** (15 mg). Fractions 47–55 (eluted with n-hexane/EtOAc (8.5:1.5), showed single upon gentle washing with *n*-hexane to afford compound **3** (21 mg). Fractions 71–88 (eluted using n-hexane/EtOAc (7.5:2.5), were combined and re-chromatographed isocratically with *n*-hexane/EtOAc (7.5:2.5) as the eluent and gave compounds **5** (7 mg) and **6** (22 mg). Fractions 127–134, eluted with n-hexane/EtOAc (7:3) were combined and further purified by gel filtration, Sephadex LH-20 (eluent: chloroform/methanol (1:1) to afford compound **1** (71 mg).

Pathogenic bacterial strains

Three Gram positive (*Staphylococcus aureus* (ATCC 25923), *Staphylococcus epidermidis* (ATCC 12228) and *Enterococcus faecalis* (ATCC 29212)) and three Gram negative (*Escherichia coli* (ATCC 25922), *Klebsiella pneumoniae* (ATCC 700603) and *Pseudomonas aeruginosa* (ATCC 27853)) bacterial strains were used to evaluate the activity of the extract and isolated compounds. The strains were obtained from the Ethiopian Public Health Institute (EPHI) and were kept in the microbiology laboratory, Traditional and Modern Medicine Research and Development Directorate, Armauer Hansen Research Institute at -78 °C in triptosoya + 20% glycerol broth.

Inoculum preparation

The inoculum size of tested bacteria was standardized according to Clinical and Laboratory Standards Institute guidelines [16]. From stored stock cultures, the bacteria were refreshed for the actual test in petri dishes containing nutrient agar by incubating for 18–24 hours at 37 °C. Test organisms were standardized by diluting with broth and measuring their absorbance using a spectrophotometer adjusted at 625 nm with an absorbance reading of optical density (OD) value range from 0.08–0.1, which is equivalent to 1.0×10^8 CFU/mL for bacteria species. The suspensions were further diluted in broth to get the final inoculum size of 5×10^5 CFU/mL [17, 18].

Evaluation of antibacterial activity

The extract and its isolated compounds were evaluated for their antibacterial activity against the selected bacterial strains using broth micro-dilution (minimum inhibitory concentration) assays as described in the literature [19-22].

The extracts and compounds (**1-6**) underwent testing to determine their minimum inhibitory concentration (MIC) through the micro-broth dilution method. Various concentrations of extracts and isolated compounds were prepared, and then introduced into the top row of 96-Micro well plates containing 100 µL of broth medium. Using multichannel micropipettes, successive two-fold dilutions were made from row A to row H. This process enabled the creation of test concentrations ranging from 25 mg/mL to 0.195 mg/mL for extracts, and from 5 mg/mL to 0.039 mg/mL for pure compounds. Subsequently, defined bacterial inoculum suspensions (5×105 CFU/mL) were added within 10-15 min of standardization. After inoculation, that is, the plates were incubated 37 °C for 18–24 hours. Then, bacterial growth corresponding to extract concentrations and pure compounds were examined after 18-24 hours of incubation. 40 µL of 0.4 mg/mL 2,3,5-triphenyltetrazolium chloride (TTC) solution was added to each 96-microwell plate and re-incubated for 30 min at 37 °C to confirm the presence or absence of purple color formation which is an indicator of microbial growth. MIC values were assessed visually using magnifying instruments. Each assay was conducted in triplicate [23]. Quality controls were carried out simultaneously in dedicated rows to ensure experiment accuracy. These included a 5% tween 80 solution as a negative control, ciprofloxacin standard as a positive control, as well as sterility and growth controls. The MIC was considered as the lowest concentration inhibiting bacterial growth under appropriate incubation conditions, expressed in mg/mL [19, 21].

Data analysis

The experiments were performed in triplicate, and the outcomes were calculated as the mean value plus or minus the standard deviation. Visual readings were taken for the results. The MIC endpoint was defined as the lowest concentration of the antibacterial substance that prevented the overall growth of microorganisms. MIC was determined based on the presence or absence of pink color using magnifying instruments.

In silico molecular docking methodology

AutoDock Vina 4.2.6 (MGL Tools 1.5.6) with standard protocol was used to dock the isolated compounds (**1**, **2**, and **3**) against downloaded protein targets such as *E. coli* DNA gyrase B (PDB ID: 6F86), *P. aeruginosa* (PDB ID: 2UV0), and *K. pneumoniae* (PDB ID: 5o79), to predict their likely binding modes of the test compounds to the target bacterial proteins [24]. The protein was prepared using the standard protocol [25, 26], which included removal of the co-crystallized ligand as well as selected water molecules and cofactors. The target protein file was prepared by leaving the associated residue with the protein by using auto-preparation of the target protein. The docking calculation results include binding energy (kcal/mol), hydrogen bond distances, and a pictorial representation of viable docked poses. ChemDraw 16.0 was used to analyze each of the 2D structures (.mol) of the isolated compounds. ChemBio3D was utilized to minimize the energy of every molecule. Through optimized structure, each molecule's 3D coordinates (PDB) were found. The docking algorithm provided with Auto Dock Vina was used to search for the best-docked conformation between ligand and protein. During the docking process, a maximum of nine conformers were considered for each ligand. The conformations with the most favorable (least) free binding energy were selected for analyzing the interactions between the target receptor and ligands by Discovery Studio Visualizer. The grid box was constructed using a docking simulation with 40 x 40 x 40 Å, pointing in x, y, and z directions, respectively, with a grid point spacing of 0.375 Å. The center grid box dimensions in XYZ directions are 61.680259, 28.330852, 64.290148 for 6F86; 39.126202, 23.661345, 54.058619 for 2UV0; and 27.311685, -12.747278, 1.635352 for 5O79. For each ligand, nine different conformations were generated and ranked based on their binding energies using AutoDock Vina functions [27]. The ligands are represented by different colors, while the H-bonds and interacting residues are represented by stick models.

In-silico drug-likeness and toxicity predictions

Bioavailability and pharmacokinetic properties were assessed to gauge their efficacy within the human body. Drug-likeness for isolated compounds (**1**, **2**, and **3**) was projected utilizing a previously established framework [28]. The structures of these compounds were translated into canonical simplified molecular-input line-entry system (SMILE) format and then subjected to SwissADME and PreADMET tools to estimate in silico pharmacokinetic parameters, including the number of hydrogen donors and acceptors, rotatable bonds, and total polar surface area [29, 39]. Factors such as solubility, skin permeability (log Kp), P-glycoprotein substrate potential, gastrointestinal permeability, and membrane permeability influence drug absorption, while distribution is governed by the blood-brain barrier (BBB), and excretion is impacted by clearance and renal OCT2 substrate [29, 31]. Cytochrome P450 (CYP) models were utilized in this evaluation. Additionally, the potential organ toxicities and toxicological endpoints of the isolated compounds were forecasted using PreADMET, ProTox-II, and OSIRIS properties. The selection of compounds as drug candidates was predicated on a parameter termed the drug score, with higher values indicating a greater likelihood of a compound being considered a viable drug candidate [29-32].

RESULTS AND DISCUSSION

The methanol extract of the root of *S. dasyphyllum* resulted in the isolation of six compounds, namely, tremulacin (**1**), scopoletin (**2**), stigmasterol (**3**), β-sitosterol (**4**), palmitic acid (**5**), and 2, 3-Dihydroxypropyl-9Z, 12Z-octadecadienoate (**6**) (Figure 1).

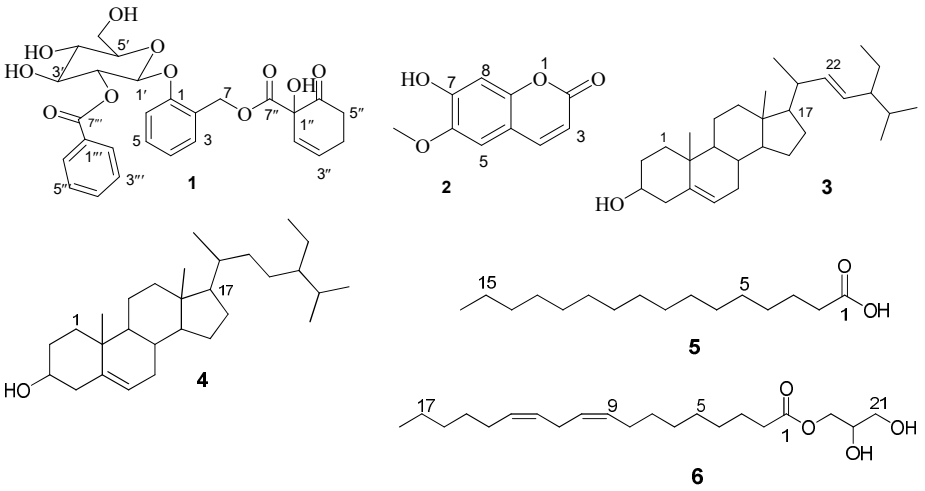

Figure 1. Chemical structure of the compounds (**1-6**) isolated from the roots of *S. dasyphyllum*.

Compound **1** was isolated as a white powder and it has a melting point of 123-125 °C. It was isolated as a major constituent of the roots of *S. dayspollum,* and its molecular formula $C_{27}H_{28}O_{11}$ was deduced from the ESI-MS indicating sodium adduct molecular ion at m/z 551 ($[M+Na]^+$). The ^{1}H NMR spectrum (500 MHz, acetone-*d6*, Table 1) showed a total of 20 proton signals assignable to three different structural units. In the downfield region, the three mutually coupled aromatic protons of ABC spin pattern centered at δ_H 8.09 (d, J = 7.9 Hz, 1H), 7.51 (t, J = 7.7 Hz, 1H) and 7.64 (t, J = 7.4 Hz, 1H) were assigned to H-2'"/H-6'", H-3-'"/H-5'", and H-4'", respectively, characteristic of a mono-substituted benzene moiety. Aromatic proton signals at δ_H 7.24 (d, J = 8.1 Hz, 1H), 7.02 (t, J = 7.4 Hz, 1H), 7.25 (t, J = 9.8 Hz, 1H) and 7.28 (d, J = 7.7 Hz, 1H) were assigned to H-3, H-4 and H-5 and H-6, respectively, indicated the presence of a 1, 2-di-substituted aromatic ring. The doublet proton at δ_H 5.76 (d, J = 9.8 Hz, 1H) and a doublet of triplet proton at δ_H 6.13 (dt, J = 9.8, 3.8, 1H) indicated the presence of olefinic protons and were assigned to H-2" and H-3", respectively. The proton signals at δ_H 5.31 (d, J = 8.2 Hz, 1H), 5.36 (t, J = 9.3 Hz, 1H), 3.96 (m, 1H), 3.69 (m, 1H), 3.70 (m, 1H) and 3.81 (m, 2H), containing HSQC correlations with carbons at δ_C 99.4 (C-1'), 74.3 (C-2'), 74.8 (C-3'), 70.6 (C-4'), 77.3 (C-5') and 61.5 (C-6'), respectively indicating the presence of phenolic glycoside. The ^{13}C NMR spectrum (Table 1) showed well resolved 27 carbons signals including seven quaternary, sixteen methine and four methylene carbons. The downfield shifted at δ_C 205.7 revealed the presence carbonyl carbon of C-6" which is twisted out of plane due to both sp^2 hybridization and to the double bond to oxygen. The others downfield shifted carbon signals that resonated at δ_C 165.3 and 169.7 indicated the presence of two ester groups attributable to carbonyl carbons of C-7'" and C-7", respectively. Comprehensive analyses of 2D NMR (^{1}H-^{1}H COSY, ^{1}H-^{13}C HMQC, and long-range HMBC) spectral data and comparison with reported literature data [33, 34], revealed that the structure of compound **1** is tremulacin. This is the first report of the isolation of this compound from *S. dasyphyllum*, having previously been reported from the leaves of *Populus trichocarpa* [33].

Compound **2** was isolated as a yellowish solid and has a melting point of 204–206 °C. The ^{1}H NMR spectrums (Table 1) showed a three-proton singlet at δ_H 3.95, indicating the presence of a methoxy group at C-6 (δ_C 56.6). Two doublet proton signals at δ_H 6.27 (1H, d, J = 9.5 Hz, H-3) and δ_H 7.60 (1H, d, J = 9.5 Hz, H-4) are the typical characteristic of conjugated olefinic protons with carbonyl of the pyrone ring in coumarin [35]. The two singlet aromatic proton signals at δ_H 6.85 (s) and δ_H 6.92 (s) are assigned to *para*-oreinted protons at C-5 and C-8, respectively, of the

tetra-substituted aromatic ring. The ^{13}C NMR spectrum (Table 1) showed well-resolved 10 carbon signals, including one carbonyl carbon at δ_C 161.6 (C-2), four protonated aromatic carbons at δ_C 113.6 (C-3), δ_C 143.4 (C-4), δ_C 107.6 (C-5), δ_C 103.4 (C-8), two oxygenated carbons at δ_C 144.2 (C-6), and 149.8 (C-7), two quaternary carbons at δ_C 151.4 (C-9), δ_C 111.7 (C-10), and δ_C 55.6 (6-O-CH_3). Based on the spectroscopic data and comparison with reported literature data [35-37], the structure of compound **2** was identified as scopoletin (7-hydroxy-6-methoxycoumarin). This is the first report of the isolation of this compound from *S. dayspollum*, having been previously reported from the leaves of *Macaranga gigantifolia* [35].

Table 1. ^1H NMR (500 MHz) and ^{13}C NMR (125 MHz) spectral data of compounds **1**, δ (ppm), in acetone-*d6)* and **2**, δ (ppm), in $CDCl_3$.

No.	Compound **1**		Compound **2**	
	δ_H (m, *J* in Hz)	δ_C	δ_H (m, *J* in Hz)	δ_C
1	-	155.0	-	-
2	-	125.0	-	161.6
3	7.24 (d, *J* = 8.1)	129.6	6.27 (d, *J* = 9.5)	113.6
4	7.02 (t, *J* = 7.4)	122.5	7.60 (d, *J* = 9.5)	143.4
5	7.25 (t, *J* = 9.8)	128.5	6.85 (s)	107.6
6	7.28 (d, *J* = 7.7)	115.5	-	144.1
7	4.95 (m), 5.15 (m)	62.3		149.7
8			6.92 (s)	103.6
9			-	150.3
10			-	111.7
11			3.95 (s)	56.6
1'	5.31 (d, *J* = 8.2)	99.4		
2'	5.36 (t, *J* = 9.3)	74.3		
3'	3.96 (m)	74.8		
4'	3.69 (m)	70.6		
5'	3.70 (m)	77.3		
6'	3.81 (m)	61.5		
1"	-	77.9		
2"	5.76 (d, *J* = 9.8)	128.3		
3"	6.13(dt, *J* = 9.8, 3.8)	131.6		
4"	2.53(m).	26.3		
5"	2.87 (m)	35.2		
6"	-	205.7		
7"	-	169.7		
1"'		130.2		
2"'	8.09 (d, *J* = 7.9)	129.6		
3"'	7.51 (t, *J* = 7.7)	128.5		
4"'	7.64 (t, *J* = 7.4)	133.2		
5"'	7.51 (m)	128.5		
6"'	8.09 (d, *J* = 7.9)	129.6		
7"'		165.3		

Compound **3** was isolated as a white solid and has a melting point of 129-131 °C. The ^{1}HNMR spectrum (Table 2) displayed the proton signals at δ_H 3.54 (dd, J = 11.1, 4.6 Hz, 1H) integrating for 1H were indicative of a hydroxymethine proton of H-3. The three doublet of doublets peaks at δ_H 5.37 (dd, J = 5.3, 1.9 Hz, 1H), 5.17 (dd, J = 15.2, 8.6 Hz, 1H), and 5.06 (dd, J = 15.2, 8.7 Hz, 1H), which are typical signals for steroidal skeleton olefinic protons of H-6, H-22, and H-23, respectively. The methyl proton signals at δ_H 1.01 (s, 3H) and 0.70 (s, 3H) correspond to H-18 and H-19. The ^{13}C NMR spectrum (Table 2) displayed 29 carbon signals, of which, three are

quaternary, eleven are methine, nine are methylene, and six are methyl, of which a hydroxyl carbon signal at δ_C 71.8 is assignable to C-3. The recognizable signals at δ_C 140.8, 121.7, 138.3, and 129.3 correspond to olefinic carbons at C-5, C-6, C-22, and C-23, respectively. Based on these spectroscopic data and comparison with the reported literature data, the structure of compound **3** was found to be stigmasterol [38, 39].

Compound **4** was also isolated as a white solid. It exhibited similar spectral features as compound **3**, including the steroidal nucleus (Table 2). The only noticeable difference is the presence of olefinic protons for H-22 (δ_H 5.17) and H-23 (δ_H 5.04) in compound **3**, and this has been missed in compound **4**. This is further supported by the ^{13}C NMR spectrum, which indicates the aliphatic nature of the carbons C-22 (δ_C 34.0) and C-23 (δ_C 26.1) in compound **4**. Therefore, the structure of compound **4** was deduced to be β-sitosterol [39]. It is highly likely that compounds **3** and **4** have been co-isolated in various plants [39, 40].

Table 2. ^{1}H NMR (500 MHz) and ^{13}C NMR (125 MHz) spectral data of compounds 3, 4, 5 and 6 δ in ppm, in $CDCl_3$.

No	Compound **3**		Compound **4**		Compound **5**		Compound **6**	
	δ_H (m, *J* in Hz)	δ_C	δ_H (m, *J* in Hz)	δ_C	δ_H (m, *J* in Hz)	δ_C	δ_H (m, *J* in Hz)	δ_C
1	1.13(m)	37.3	-	37.3	-	178.6	-	174.3
2	1.85(m)	31.7		31.7	2.37 (t, *J* = 7.5)	33.8	2.37 (t, J = 5.0 Hz)	34.1
3	3.54 (dd, *J* = 11.1, 4.6)	71.8	3.55 (m, *J* = 11.1, 4.6)	71.8	1.65 (q, *J* = 7.4)	24.7	1.69 – 1.62 (m)	24.9
4	2.28(m)	42.3	2.26(m)	42.3	1.28 (m)	29.7	1.33(m)	29.4
5	-	140.8	-	140.8	1.28 (m)	29.6	1.33(m)	29.7
6	5.37 (dd, *J* = 5.3, 1.9)	121.7	5.37 (d *J* = 4.4, 1.8)	121.7	1.28 (m)	29.6	1.33(m)	29.7
7	1.99 (m)	31.9	1.98 (m)	31.9	1.28 (m,)	29.4	1.33(m)	31.5
8	1.55(m)	29.2	1.53(m)	29.2	1.28 (m)	29.7	2.07 (m)	27.2
9	0.93(m)	50.2	0.94(m)	50.1	1.28 (m)	29.7	5.51–5.24 (m)	128.1
10	-	36.5	-	36.5	1.28 (m)	29.7	5.51–5.24 (m)	130.2
11	1.43(m)	21.1	1.43(m)	21.1	1.28 (m)	29.4	2.79(m)	25.6
12	1.48(m)	39.9	1.48(m)	39.8	1.28 (m)	29.2	5.51–5.24 (m)	130.0
13	-	42.2	-	42.3	1.28 (m)	29.1	5.51–5.24 (m)	127.9
14	1.06(m)	56.9	1.06(m)	56.8	1.28 (m)	31.9	1.33(m)	29.1
15	1.59(m)	24.4	1.59(m)	24.3	1.32 m)	22.7	1.33(m)	29.6
16	1.29(m)	28.9	1.28(m)	28.3	0.90 (t, *J* = 6.8)	14.1	1.33(m)	31.9
17	1.17(m)	56.0	1.16(m)	56.1			1.33(m)	22.7
18	0.70 (s)	12.4	0.70(s)	11.9			0.90 (t, J = 6.8)	14.8
19	1.01 (s)	19.1	0.87 (s)	18.8			4.23 (dd, J = 11.7, 4.6)	65.2
20	2.06(m)	40.5	1.35(m)	36.2			3.97(m)	70.3
21	1.04(m)	21.3	0.94(m)	19.0			3.64 (dd, *J* = 4.9, 1.4)	63.3
22	5.17 (dd, *J* = 15.2, 8.6)	138.3	1.28 (m)	34.0				
23	5.04 (dd, *J* = 15.2, 8.7)	129.3	1.18 (m)	26.1				
24	1.54(m)	51.3	0.95 (m)	45.8				
25	1.44(m)	31.9	1.67(m)	31.9				
26	0.84 (m)	21.1	0.84 (m)	19.8				
27	0.86(m)	19.6	0.86(t)	19.4				
28	1.07(m)	25.4	1.20(m)	23.1				
29	0.83(m)	12.2	0.83(t)	12.0				

Compound **5** was obtained as a white solid. The ^{1}H NMR spectrum (Table 2) revealed typical characteristic signals for long chains of fatty acid derivatives that showed triplet protons at δ_H 2.37 (t, J = 7.5 Hz, 2H) for protons adjacent to the carbonyl group and another quintet proton signal at δ_H 1.65 (q, J = 7.4 Hz, 2H) attributed to protons at C-3 (δ_C 24.7). Moreover, the overlapped multiple peaks in the interval of δ_H 1.28–1.32 are also typical properties of aliphatic protons, which are integrated for twenty-four protons. The up-field shifted triplet signal at δ_H 0.90 (t, J = 6.8 Hz, 3H) designated the presence of terminal methyl protons at C-16 [35]. The singlet at δH 10.38 was indicative of the presence of carboxylic acid. The ^{13}C NMR spectrum (Table 2) showed signals for 16 carbon atoms, including the carbon signal resonating at δ_C 178.6 for the carbonyl of the carboxylic group. The close-range carbon signals from δ_C 29.1–29.7 indicate the long-chain methylene groups (CH_2). Based on these spectroscopic observations and comparisons with literature data [41, 42], the structure of compound **5** was identified as hexadecanoic acid or palmitic acid.

Compound **6** was isolated as white viscous oil. The ^{1}H NMR spectrum in $CDCl_3$ (Table 2) showed characteristic peaks for long-chain fatty acid derivatives. It also further showed downfield shifted chemical shift values at δ_H 5.51–5.24 (m) for H-9, H-10, H-12, and H-13. The triplet peak at δ_H 2.37 (t, J = 5.0 Hz) for two protons is attributed to the protons adjacent to the carbonyl group. The up-field signal in the ^{1}H NMR spectrum at δ_H 0.90 (t, J = 6.8 Hz) indicated the presence of terminal methyl protons. The doublet of doublet peaks at δ_H 4.23 (dd, J = 11.7, 4.6 Hz) and at δ_H 3.64 (dd, *J* = 4.9, 1.4 Hz) are due to nonequivalent geminal protons at C-19 (δ_C 65.2) and C-21 (δ_C 63.3), respectively. The ^{13}C NMR (Table 2) spectrum showed the presence of well-resolved signals for 21 carbon atoms. The downfield shifted the carbon signal at δ_C 174.3 (C-1), indicating the presence of carbonyl carbon for the ester moiety. The presence of four olefinic carbon signals at δ_C 130.2 (C-10), 130.0 (C-12), 128.1 (C-9), and 127.9 (C-13) were also evident. Additionally, twelve methylene carbons (δ_C 22.6–34.2) and a methyl carbon (δ_C 14.1) were confirmed from the ^{13}C-NMR spectrum. Based on this spectroscopic information and comparisons with literature data [43, 44], the structure of compound **6** was identified as 2,3-dihydroxypropyl 9Z, 12Z-octadecadienoate. This compound has previously been reported from the leaves of *Sasa quelpaertensis* [43].

Antibacterial activity

The antibacterial activity of the extract and isolated compounds was examined using the micro-dilution method against three Gram-positive and three Gram-negative bacterial strains (Table 3). These strains are among the pathogenic bacterial strains that are resistant to the majority of first-line medications [45]. Both the extract and isolated compounds demonstrated antibacterial activity, with varying degrees of responses against the bacterial strains. The crude extract showed considerable activity against bacterial strains, with a minimum inhibition concentration (MIC) ranging from 0.195±0.0 to 6.250±0.0 mg/mL. The highest activity with a MIC value of 0.195±0.0 mg/mL was observed against *S. epidermidis, E. coli*, and *P. aerogenosa* bacterial strains. Additionally, it demonstrated promising activity against *S. aureus* and *K. pneumoniae* bacteria, with MIC values of 0.391±0.0 mg/mL.

Despite differences in activity, all test bacterial species were susceptible to all compounds, though their activity varied. Compound **2** showed the highest antibacterial activity; with MIC values of 0.313±0.0 mg/mL against *K. pneumoniae* and 0.625±0.0 mg/mL against both *E. coli* and *P. aeruginosa* (see Table 3). Encouraging activity was observed for compounds **1**, and **3** against *K. pneumoniae* with MIC values of 1.25±0.0 mg/mL. In contrast, compounds **4**, **5**, and **6** demonstrated medium to low potency against the test bacterial strains.

Overall, the isolated compounds displayed somewhat lower antibacterial activity against all tested bacteria compared to the crude root extracts. The enhanced antibacterial effects of the crude extracts are likely due to the synergistic interactions among their various components. This is

supported by the presence of phytochemicals in the plant, including flavonoids, alkaloids, saponins, cyanogenic glycosides, tannins, and reducing sugars [12]. Previous reports on the antimicrobial properties of the methanolic extract and it's fractions also demonstrated significant antibacterial activity [12]. These findings affirm the traditional use of the plant [9, 12, 13] and highlight its potential as a valuable resource for developing new antibacterial agents [46].

Table 3. MIC values of the crude extract and isolated compounds (in mg/mL) against tested microorganisms.

Bacteria strains	Extract	Average MIC values from triplicate assays of the compounds and reference drug						
		1	**2**	**3**	**4**	**5**	**6**	Cipro.
S. aureus	0.391±0.0	2.50±0.0	2.50±0.0	5.00±0.0	5.0±0.0	5.00±0.0	2.50±0.0	0.313±0.0
S. epider.	0.195±0.0	2.50±0.0	2.50±0.0	5.00±0.0	2.50±0.0	5.00±0.0	5.00±0.0	0.156±0.0
E. faecalis	6.25±0.0	2.50±0.0	2.50±0.0	2.50±0.0	5.00±0.0	5.00±0.0	2.50±0.0	0.313±0.0
E. coli	0.195±0.0	2.50±0.0	0.625±0.0	5.00±0.0	2.50±0.0	2.50±0.0	>□.00	0.078±0.0
K. pneum.	0.391±0.0	1.25±0.0	0.313±0.0	1.25±0.0	2.50±0.0	2.50±0.0	>□.00	0.195±0.0
P. aerug.	0.195±0.0	2.50±0.0	0.625±0.0	5.00±0.0	5.00±0.0	5.00±0.0	5.00±0.0	0.039±0.0

Key: *S. epider = S. epidermidis, K. pneum = K. pneumoniae, P. aerug = P. aeruginosa,* Cipro = Ciprofloxacin is a positive control drug. Each value represents the mean value from triplicate assays.

Molecular docking analysis

In association with i*n vitro* antibacterial activity, the molecular docking study was carried out to assess the binding affinity and binding interactions of isolated compounds (**1–3**) toward target proteins: *E. coli* DNA gyrase B (PDB ID: 6F86), *P. aeruginosa* (PDB ID: 2UV0), and *K. pneumoniae* (PDB ID: 5o79). The Protein Data Bank (PDB) provided the protein crystal structures. In the AutoDock Vina platform, a ligand-target complex with a higher negative value denotes better binding between the ligand and its target proteins. The binding affinity, bonding interactions, and residual amino acid interactions of compounds and ciprofloxacin are summarized in Tables 4 and 5.

Compounds **1** and **3** showed the highest binding affinities against *K. pneumoniae*, with values of -8.9 and -8.7 kcal/mol, respectively, surpassing the standard drug ciprofloxacin, which has a binding affinity of -7.9 kcal/mol. Compound **2** with a binding affinity of -7.1 kcal/mol against the same strain, shows slightly lower affinity compared to ciprofloxacin. However, Compound **2** demonstrated a better binding affinity to the LasR protein of *P. aeruginosa* (-7.1 kcal/mol) compared to ciprofloxacin (-6.5 kcal/mol), though it showed a slightly lower affinity for *E. coli* DNA gyrase B (-5.5 kcal/mol) compared to ciprofloxacin (-6.9 kcal/mol). These low docking scores reflect strong interactions of the compounds with the protein-binding pockets.

The study demonstrated that the isolated compounds exhibited H-bonding, hydrophobic, and van der Waals interactions with binding pockets of *K. pneumoniae, E. coli* DNA gyrase B, and *P. aeruginosa.* AutoDock Vina was also used to map the amino acid residues involved in hydrogen bonds, hydrophobic interactions, and van der Waals interactions at each ligand-protein complex (Figures 2–4). Overall, the results obtained from the molecular docking study for these compounds **1**, **2**, and **3** agreed with the *in vitro* antibacterial activity against *E. coli* DNA gyrase B, *P. aeruginosa*, and *K. pneumoniae*.

Table 4. Molecular docking results of compounds **1**, **2**, and **3** against *K. pneumoniae* (PDB ID: 5079).

Ligands/ Compounds	Binding Affinity (Kcal/Mol)	H-Bond	Residual Interactions	
			Hydrophobic and Electrostatic	Van Der Waals
1 ($C_{27}H_{28}O_{11}$)	-8.9	Lys-16, Tyr-35, Arg-37, Arg-37, Glu-110	Hydrophobic -Pi-Pi Stacked- Phe-111, Hydrophobic- Pi-Pi T-shaped- Tyr-35 Hydrophobic Pi-Alkyl- Val-29, Hydrophobic- Pi-Alkyl -Val-335	Asp-18, Tyr-22, Asn-59, Gln-61, Trp-73, Leu-108, Pro-109, Tyr-311, Lys-315
2 ($C_{10}H_8O_4$)	-7.1	Leu-340	Hydrophobic Pi-Pi Stacked-Tyr-91, Hydrophobic Alkyl-Leu-340, Hydrophobic Pi-Alkyl-Phe-89, Hydrophobic Pi-Alkyl-Leu-338, Hydrophobic Pi-Alkyl-Ala-130	Tyr-150, Phe-23, His-21, Gly-19, Gly-339, Leu-20
3 ($C_{29}H_{48}O$)	-8.7	-	Hydrophobic Pi-Sigma-Phe-89, Hydrophobic Alkyl-Ala-130, Hydrophobic Alkyl-Leu-338, Hydrophobic Alkyl-Leu-340, Hydrophobic Pi-Alkyl-Phe-89, Hydrophobic Pi-Alkyl-Tyr-91, Hydrophobic Pi-Alkyl-His-21	Thr-310, Leu-81, Phe-83, Phe-23
Ciprofloxacin ($C_{17}H_{18}FN_3O_3$)	-7.9	Leu-338	Hydrophobic Pi-Sigma-Leu-338, Hydrophobic Pi-Pi Stacked-Phe-89, Hydrophobic Pi-Pi Stacked-Tyr-91, Hydrophobic Alkyl-Leu-338, Hydrophobic Pi-Alkyl-Phe-89, Hydrophobic Pi-Alkyl-Leu3-38 Hydrophobic Pi-Alkyl-Leu-340	Phe-304, Leu-81, Phe-83, Thr-310, Gly-19, Gly-339, Leu-20, His-21

Table 5. Molecular docking result of compound 2 against *E. coli* DNA gyrase B (PDB ID: 6F86) and LasR protein of *P. aeruginosa* (PDB ID: 2UV0).

Ligands/ compounds	Binding affinity (kcal/Mol)	H-Bond	Residual interactions	
			Hydrophobic and electrostatic	Van Der Waals
E. coli DNA gyrase B (PDB ID: 6F86)				
2 ($C_{10}H_8O_4$)	-5.5	Gly-77	Electrostatic Pi-Anion-Glu-50, Hydrophobic Alkyl-Ile-94, Hydrophobic Pi-Alkyl-Ile-78	Asn-46, Pro-79, Arg-76, Gly-164, Gly-75, Thr-165, Asp-73
Ciprofloxacin ($C_{17}H_{18}FN_3O_3$)	-6.9	Gly-77, Asn-46	Halogen (Fluorine)-Arg-76, Halogen (Fluorine)-Gly-77, Electrostatic Pi-Cation-Arg-76, Electrostatic Pi-Anion-Glu-50, Hydrophobic Alkyl-Pro-79, Hydrophobic Pi-Alkyl-Ile-78, Hydrophobic Pi-Alkyl-Arg-76, Hydrophobic Pi-Alkyl-Pro-79	Ala-47, Thr-165, Gly-75, Arg-136
LasR protein of *P. aeruginosa* (PDB ID: 2UV0)				
2 ($C_{10}H_8O_4$)	-7.1	Tyr-56	Electrostatic Pi-Anion-Asp-73, Hydrophobic Pi-Sigma-Leu-36, Hydrophobic Pi-Pi Stacked-Tyr-64	Leu-110, Arg-61, Ile-52, Asp-65, Gly-38, Thr-

			Hydrophobic Alkyl-Ala-70, Hydrophobic Alkyl-Val-76, Hydrophobic Pi-Alkyl-Tyr-47, Hydrophobic Pi-Alkyl-Val-76, Hydrophobic Pi-Alkyl-Ala-127, Hydrophobic Pi-Alkyl-Leu-36, Hydrophobic Pi-Alkyl-Ala-127	75,Thr-115, Ser-129, Trp-88
Ciprofloxacin ($C_{17}H_{18}FN_3O_3$)	-6.5	Lys-42, Asp-43, Tyr-47, Asp-43	Electrostatic Pi-Anion-Asp-43, Hydrophobic Alkyl-Arg-122, Hydrophobic Pi-Alkyl-Leu-125	Gly-123, Thr-80, Gln-45, Ser-44, Lys-42

In silico pharmacokinetics (drug-likeness) and toxicity analysis

The structures of isolated compounds (**1-3**) were converted to their canonical simplified molecular-input line-entry system (SMILE) and submitted to the SwissADME tool to estimate *in silico* pharmacokinetic parameters (drug-likeness properties) according to Lipinski's rule of five [24, 28] and Veber's rule [47]. Lipinski's rule of five implies that the drugs and/or candidates should obey the five-parameter rule, which states that hydrogen-bond donors (NHDs) should be less than 5, hydrogen-bond acceptors (NHAs) should be less than 10, molecular mass should be less than (MW) 500 Daltons, and log P should be less than 5. This could be a good drug candidate. According to Veber's rule, a compound with rotatable bonds (RTB) < 10 and a polar surface area (TPSA) < 140 $Å^2$ should present good oral bioavailability. Drug-likeness is a prediction that screens whether a particular organic molecule has properties consistent with being an orally active drug [28, 47, 48]. The SwissADME prediction outcome showed that compound **2** satisfies Lipinski's rule of five with zero violations. The hydrogen bonding potential and bioavailability of molecules are closely correlated to the TPSA value. Thus, the TPSA value of compound **2** was noticed as 59.67 $Å^2$ and is well below the limit of 140 $Å^2$ (Table 6). The calculated numbers of rotatable bonds (NRB) values for compound **2** are less than 10, which indicates the compound is conformationally stable. The absorption, distribution, metabolism, excretion, and toxicity (ADMET) studies of isolated compounds (**1-3**) were also predicted using Swiss ADMET (Table 6). The skin permeability value (Kp) in cm/s indicates the skin absorption of molecules [49]. The skin permeability (Kp) values of the compounds ranged from -2.74 to -8.32 cm/s, suggesting computable moderate skin permeability and places them close to the permeability range of the broad-spectrum antibiotic ciprofloxacin, which has a Kp value of -9.09 cm/s. The Swiss ADME prediction indicated that compound **2** showed high gastrointestinal (GI) absorption and blood-brain barrier (BBB) permeation, whereas compounds 1 and 3 displayed low absorption and blood-brain barrier (BBB). The toxicity profiles of the studied compound were carried out using ProTox-II and OSIRIS Property Explorer. Acute toxicity prediction results, such as toxicity class classification and LD_{50} values, predict that none of the isolated compounds has acute toxicity (LD_{50} > 5000, toxicity class > 5) (Table 6). The ProTox-II prediction of the toxicological prediction gives results for endpoints such as hepatotoxicity, carcinogenicity, immunotoxicity, mutagenicity, and cytotoxicity. Compound **2** demonstrated active carcinogenicity, despite the studied compounds' predicted non-carcinogenic and non-irritating properties. All of the compounds, however, exhibited no action against cytotoxicity, mutagenicity, or hepatotoxicity.

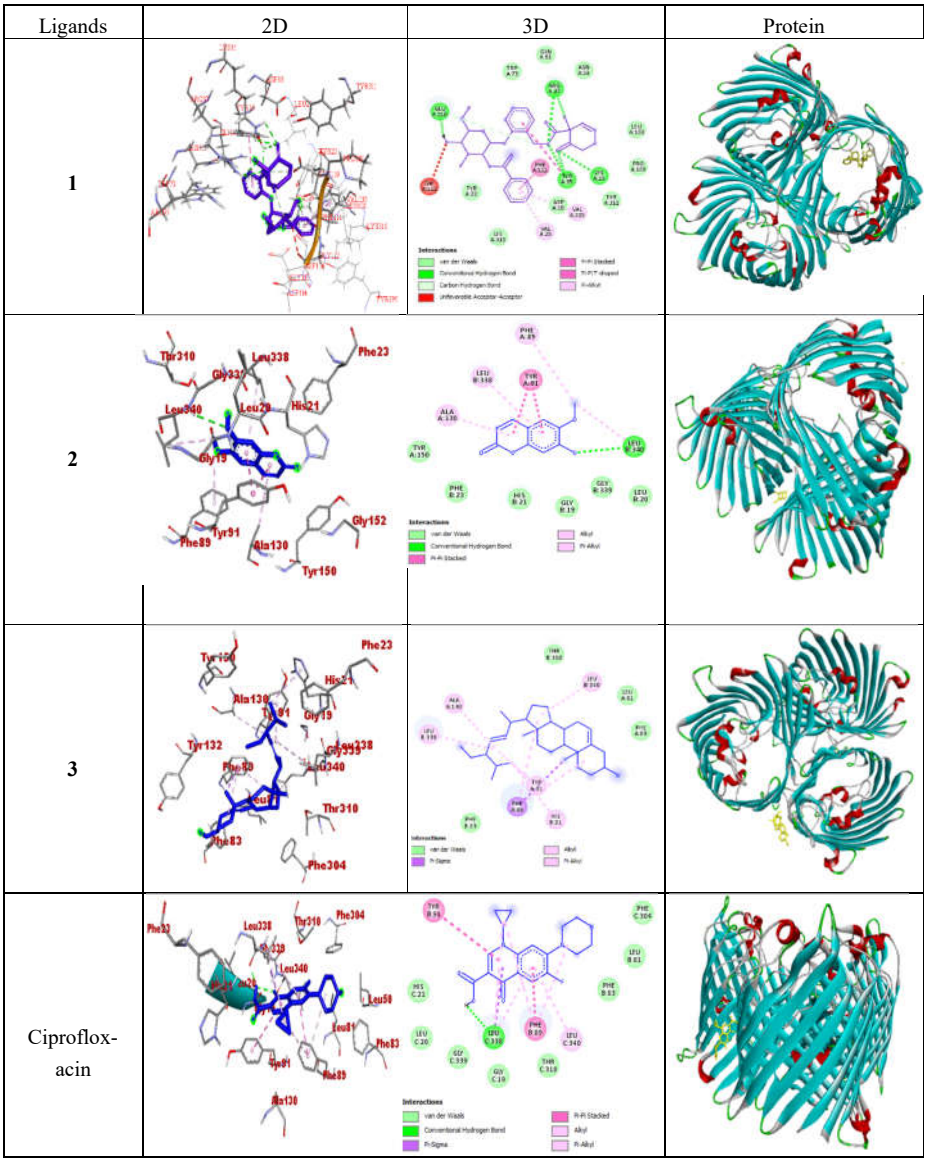

Figure 2. 2D (middle), 3D (left), and protein (right) binding interactions of compound **1**, **2**, **3** and ciprofloxacin against *K. pneumoniae* Ompk36 (PDB ID: 5O79).

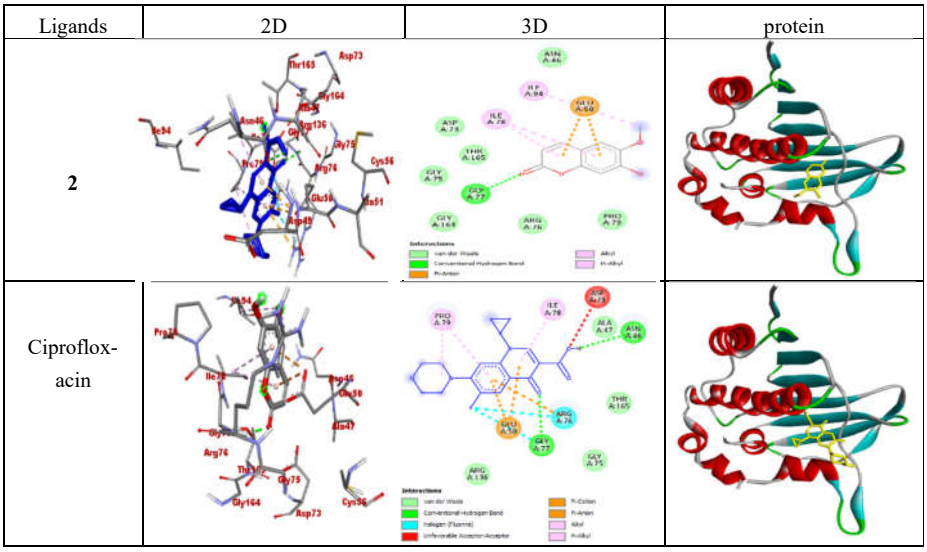

Figure 3. 2D (middle), 3D (left) and protein (right) binding interactions of compound **2** and ciprofloxacin against *E. coli* DNA gyrase B (PDB ID: 6F86).

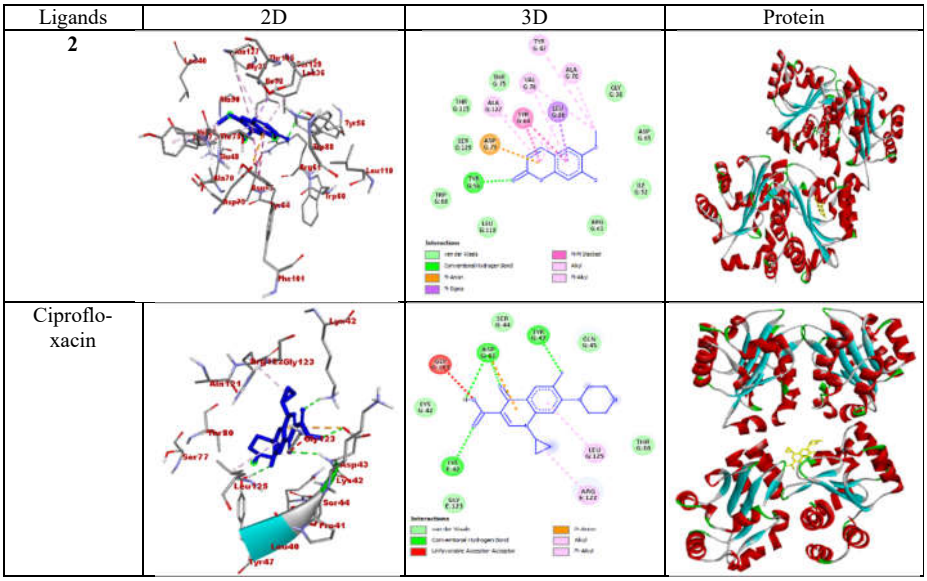

Figure 4. 2D (middle), 3D (left), and protein (right) binding interactions of compound **2** and ciprofloxacin against LasR protein of *P. aeruginosa* (PDB ID: 2UV0).

Table 6. *In Silico* Drug-Likeness, ADME and Toxicity Predictions of compounds 1–3 and ciprofloxacin using SwissADME, PreADMET, ProTox-II, and OSIRIS Property Explorer.

Predicted parameters			Compounds			
			1	**2**	**3**	Ciprofloxacin
Drug likeness	MF		$C_{27}H_{28}O_{11}$	$C_{10}H_8O_4$	$C_{29}H_{48}O$	$C_{17}H_{18}FN_3O_3$
	MW (g/mol)		528.5	192.17	412.69	331.34
	NHD		4	1	1	2
	NHA		11	4	1	5
	NRB		10	1	5	3
	TPSA(Å^2)		128.94	59.67	20.23	74.57
	LogP (iLogP) Lipophilicity		3.93	1.86	5.01	2.24
	Log P (MLOGP) Lipophilicity		-06	0.76	6.62	1.28
	Log S (ESOL) Water Solubility		-3.76	-2.46	-7.46	-1.32
	Lipinski's rule of five violations		2	0	1	0
ADME predictions	Skin Permeation (Log Kp) cm/s		-8.32	-6.39	-2.74	-9.09
	GIA Absorption		Low	High	Low	High
	BBB Permeability		No	Yes	No	No
	Inhibitor Interaction	P-gp substrate	Yes	No	No	Yes
		CYP1A2	No	Yes	No	No
		CYP2C19	No	No	No	No
		CYP2C9	No	No	Yes	No
		CYP2D6	No	No	No	No
		CYP3A4	No	No	No	No
Toxicity prediction	LD_{50} (mg/kg)		5000	3800	890	2000
	Toxicity Class		5	5	4	4
	Organ Toxicity	Hepatotoxicity	Inactive	Inactive	Inactive	Inactive
		Carcinogenicity	Inactive	active	Inactive	Inactive
		Immunotoxicity	active	active	active	Inactive
		Mutagenicity	Inactive	Inactive	Inactive	active
		Cytotoxicity	Inactive	Inactive	Inactive	Inactive
		Irritant	No	No	No	No

Key: NHD = number of hydrogen donors, NHA = number of hydrogen acceptors, NRB = number of rotatable bonds, and TPSA = total polar surface area, GI = gastrointestinal, BBB = blood brain barrier, P-gp = P-glycoprotein, and CYP = cytochrome.

CONCLUSIONS

The chromatographic separation of the root extract of *S. dasyphyllum* led to the isolation of tremulacin (**1**), scopoletin (**2**), stigmasterol (**3**), β-sitosterol (**4**), palmitic acid (**5**), and 2,3-dihydroxypropyl 9Z,12Z-octadecadienoate (**6**). The crude extract and the isolated compounds demonstrated promising antibacterial activity against the tested strains. The crude extracts exhibited stronger antibacterial activity against *S. epidermidis*, *E. coli*, and *P. aeruginosa* with the same MIC values of 0.195±0.0 mg/mL. Among the isolated compounds, the highest antibacterial activities were recorded for compound **2**, with MIC values of 0.313±0.0 mg/mL against *K. pneumoniae* and 0.625±0.0 mg/mL against both *E. coli* and *P. aeruginosa. In silico* molecular docking analyses revealed promising scoring poses with compounds 1-3 had minimum binding energies against *K. pneumoniae*. Furthermore, compounds **1** and **2** showed the highest drug-likeness characteristics, indicating that these compounds have both remarkable biological activities and the potential to function as drugs. The traditional uses of *S. dasyphyllum* roots are

supported by experimental studies that indicate the potential use of isolated compounds as potential drug leads. However, it is advised to conduct further exhaustive evaluations, including *in vivo* antibacterial activity tests, in order to make a conclusive decision regarding the plant's potential for formulation and medical applications.

ACKNOWLEDGMENTS

The authors are thankful for the facilities provided by the Traditional and Modern Medicine Research and Development Directorate, Armauer Hansen Research Institute, Addis Ababa, Ethiopia. Mr. Dereilo Bekere extends his gratitude to Wollega University, Ethiopia, for the financial support provided.

REFERENCES

1. Kaunda, J.S.; Zhang, Y.J. The genus solanum: An ethnopharmacological, phytochemical and biological properties review. *Nat. Prod. Bioprospect*. **2019**, 9, 77-137.
2. Muthoni, J.; Shimelis, H.; Melis, R.; Kabira, J. Reproductive biology and early generation's selection in conventional potato breeding. *Aust. J. Crop Sci.* **2012**, 6, 488-97.
3. Contreras-Angulo, L.; Emus-Medina, A.; Gutierrez-Grijalva, E.; Ambriz-Pérez, D.; Elizalde-Romero, C.; Heredia, J.B. Pharmacological potential of Solanum genus. Solanum: An Overview. *Plant Sci. Res*. **2020**, 1, 199.
4. Gürbüz, N.; Uluişik, S.; Frary, A.; Frary, A.; Doğanlar, S. Health benefits and bioactive compounds of eggplant. *Food Chem*. **2018**, 268, 602-610.
5. Scorsatto, M.; Rosa, G.; Raggio Luiz, R.; da Rocha Pinheiro Mulder, A.; Junger Teodoro, A.; Moraes de Oliveira, G.M. Effect of eggplant flour (*Solanum melongena* L.) associated with hypoenergetic diet on antioxidant status in overweight women-a randomised clinical trial. *Int. J. Food Sci.* **2019**, 54, 2182-2189.
6. Gbile, Z.O.; Adesina, S.K. Nigerian Solanum species of economic importance. *Ann. Missouri Botan. Garden.* **1988**, 75, 862-865.
7. Paulos, B.; Fenta, T. G.; Bisrat, D.; Asres, K. Health seeking behavior and use of medicinal plants among the Hamer ethnic group, South Omo zone, southwestern Ethiopia. *J. Ethnobiol. Ethnomed.* **2016**, 12, 1-13.
8. Funmilola, A.R.; Abubakar, G.; Hassan, Z. In-vitro antivenom potential of *Solanum dasyphyllum* methanolic leaf and fruit extracts against Naja nigricollis venom. *Eur. J. Med. Plants.* **2020**, 31, 38-45.
9. Oyinloye, O.E.; Ajayi, A.M.; Ademowo, O.G. *Solanum dasyphyllum* leaf extract reduces inflammation in carrageenan-induced air pouch in rats by inhibition of cyclooxygenase-2 and inducible nitric oxide synthase. *Nutrire* **2022**, 47, 1-11.
10. Kitata, G.; Abdeta, D.; Amante, M. Ethnoknowledge of plants used in veterinary practices in Midakegn district, west showa of Oromia region, Ethiopia. population. *J. Med. Plan. Stud.* **2017**, 5, 282-288.
11. Sodeinde, O.A.; Salawu, K.M.; Ogbole, O.O.; Ajaiyeoba, E.O. Phytochemical, antioxidant, brine shrimp lethality and antiproliferative analyses of *Solanum dasyphyllum* schum. and thonn. leaf and fruit extracts [Solanaceae]. *Savannah Vet. J.* **2019**, 13-17.
12. Oyinloye, O.E.; Alabi, O.S.; Ademowo, O.G. GC-MS profiling and evaluation of antioxidant and antimicrobial properties of methanolic extract and fractions of the leaves of *Solanum dasyphyllum* Schumach and Thonn. *West Afr. J. Med*. **2023**, 34, 22-41.
13. Oyinloye, O.E.; Ajayi, A.M.; Ademowo, O.G. Phytochemical analysis and anti-inflammatory activity of *Solanum dasyphyllum* Schumach. and Thonn. Leaves methanol extract and its fractions. *Trop. J. Nat. Prod. Res*. **2021**, 5, 2165-2169.

14. Obade, E.; Ilesanmi, O.B.; Crown, O.; Akinmoladun, A.C.; Olaleye, T.M.; Akindahunsi, A.A. Neuromodulatory effect of solvent fractions of Africa eggplant (*Solanium dadyphyllum*) against KCN-induced mitochondria damage, viz. NADH-succinate dehydrogenase, NADH-cytochrome c reductase, and succinate-cytochrome c reductase. *Clin. Phytosci.* **2018**, 4, 1-9.
15. Ilesanmi, O.B.; Efe, O.; Odewale, T.T.; Atanu, F.O.; Adeogun, E.F.; Akinmoladun, A.C.; Olaleye, T.M. Reversal effect of against rotenone-induced neurotoxicity. *Curr. Issues Pharm. Med. Sci.* **2020**, 33, 191-196.
16. Wayne, P. Clinical and laboratory standards institute. Performance standards for antimicrobial susceptibility testing. *Inform. Supp*. **2011**, 3, 100-121.
17. Al-Salt, J. Antimicrobial activity of crude extracts of some plant leaves. *Res. J.microbiol.* **2012**, 7, 59-37.
18. Huse, H.K.; Miller, S.A.; Chandrasekaran, S.; Hindler, J.A.; Lawhon, S.D.; Bemis, D.A.; Westblade, L.F.; Humphries, R.M. Evaluation of oxacillin and cefoxitin disk diffusion and MIC breakpoints established by the clinical and laboratory standards institute for detection of mecA-mediated oxacillin resistance in Staphylococcus schleiferi. *J. Clin. Microbiol.* **2018**, 56, e01653-17.
19. Eloff, J.N. A sensitive and quick microplate method to determine the minimal inhibitory concentration of plant extracts for bacteria. *Planta Med*. **1998**, 64, 711-713.
20. Wayne, R.O. *Plant Cell Biology: From Astronomy to Zoology*. Academic Press: New York; **2009**.
21. Weinstein, M.P.; Lewis, J.S. The clinical and laboratory standards institute subcommittee on antimicrobial susceptibility testing: Background, organization, functions, and processes. *J. Clin. Microbiol.* **2020**, 58, 01864-19.
22. Humphries, R.; Bobenchik, A.M.; Hindler, J.A.; Schuetz, A.N. Overview of changes to the clinical and laboratory standards institute performance standards for antimicrobial susceptibility testing, M100. *J. Clin. Microbiol.* **2021**, 59, e0021321.
23. Mostafa, A.A.; Al-Askar, A.A.; Almaary, K.S.; Dawoud, T.M.; Sholkamy, E.N.; Bakri, M.M. Antimicrobial activity of some plant extracts against bacterial strains causing food poisoning diseases. *Saudi J. Biol. Sci*. **2018**, 25, 361-366.
24. Trott, O.; Olson, A.J. AutoDock Vina: improving the speed and accuracy of docking with a new scoring function, efficient optimization, and multithreading. *J. Comput. Chem.* **2010**, 31, 455-461.
25. Müller, I. Guidelines for the successful generation of protein–ligand complex crystals. *Acta Cryst*. **2017**, 73, 79-92.
26. Baby, S.T.; Sharma, S.; Enaganti, S.; Cherian, P.R. Molecular docking and pharmacophore studies of heterocyclic compounds as Heat shock protein 90 (Hsp90) Inhibitors. *Bioinformatics* **2016**, 12, 149.
27. Melaku, Y.; Getahun, T.; Addisu, M.; Tesso, H.; Eswaramoorthy, R.; Garg, A. Molecular docking, antibacterial and antioxidant activities of compounds isolated from Ethiopian plants. *Int. J. Second. Metab.* **2022**, 9, 208-328.
28. Lipinski, C.A.; Lombardo, F.; Dominy, B.W.; Feeney, P.J. Experimental and computational approaches to estimate solubility and permeability in drug discovery and development settings. *Adv. Drug Deliv. Rev*. **1997**, 23, 3-25.
29. Jia, C.Y.; Li, J.Y.; Hao, G.F.; Yang, G.F. A drug-likeness toolbox facilitates ADMET study in drug discovery. *Drug Discov. Today* **2020**, 25, 248-258.
30. Kar, S.; Leszczynski, J. Open access in silico tools to predict the ADMET profiling of drug candidates. *Expert Opin. Drug Discov.* **2020**, 15, 1473-1487.
31. Mahanthesh, M.T.; Ranjith, D.; Yaligar, R.; Jyothi, R.; Narappa, G; Ravi, M. V. Swiss ADME prediction of phytochemicals present in *Butea monosperma* (Lam.) *Taub. J. Pharmacogn. Phytochem.* **2020**, 9, 1799-809.

32. Meanwell, N.A. Improving drug candidates by design: a focus on physicochemical properties as a means of improving compound disposition and safety. *Chem. Res. Toxicol.* **2011**, 24, 1420-1456.
33. Feistel, F.; Paetz, C.; Lorenz, S.; Schneider, B. The absolute configuration of salicortin, HCH-salicortin and tremulacin from Populus trichocarpa× deltoides Beaupré. *Molecules* **2015**, 20, 5566-5573.
34. Ishikawa, T.; Nishigaya, K.; Takami, K.; Uchikoshi, H.; Chen, I.S.; Tsai, I.L. Isolation of salicin derivatives from homalium c ochinchinensis and their antiviral activities. *J. Nat. Prod.* **2004**, 67, 659-663.
35. Darmawan, A.; Kosela, S.; Kardono, L.B.; Syah, Y.M. Scopoletin, a coumarin derivative compound isolated from *Macaranga gigantifolia* Merr. *J. App. Pharm. Sci*. **2012**, 2, 175-177.
36. Shah, M.R.; Shamim, A.; White, L.S.; Bertino, M.F.; Mesaik, M.A.; Soomro, S. The anti-inflammatory properties of Au–scopoletin nanoconjugates. *New J. Chem.* **2014**, 38, 5566-5572.
37. Tatke, P.; Rajan, M. Comparison of conventional and novel extraction techniques for the extraction of scopoletin from *Convolvulus pluricaulis. Indian J. Pharm. Educ. Res.* **2014**, 48, 27-31.
38. Talla, E.; Yankep, E.; Mbafor, J.T. Chemical constituents from root barks of *Erythrina mildbraedii* and stem barks of *Erythrina addisoniae*. *Bull. Chem. Soc. Ethiop*. **2014**, 28, 155-159.
39. Erwin, E.; Pusparohmana, W.R.; Safitry, R.D.; Marliana, E.; Usman, E.; Kusuma, I.W. Isolation and characterization of stigmasterol and β-sitosterol from wood bark extract of Baccaurea macrocarpa Miq. Mull. Arg. *Rasāyan J. Chem*. **2020**, 13, 2552-2558.
40. Emam, J.A.; Yaya, E.E.; Choudhary, M.I.; Yousuf, S.; Gebremedihn, T.M. In vitro antifungal, anti-inflammatory and cytotoxic activities of *Rumex abyssinicus* rhizome extract and bioassay-guided isolation of cytotoxic compounds from Rumex abyssinicus. *Bull. Chem. Soc. Ethiop*. **2022**, 36, 879-892.
41. Bulama, J.; Dangoggo, S.; Halilu, M.; Tsafe, A.I.; Hassan, S.W. Isolation and characterization of palmitic acid from ethyl acetate extract of root bark of *Terminalia glaucescens*. *Chem. Mat. Res*. **2014**, 6, 140-144.
42. Ekeocha, P.A.; Ezeh, C.O.; Anyam, J.V.; Onyekwelu, K.C.; Ikekpeazu, J.; Igoli, J.O. Isolation, structural elucidation and therapeutic potentials of root of *Cucurbita pepo*. *Indian J. Pharm. Sci*. **2021**, 83, 1288-1294.
43. Ko, H.C.; Jang, M.G.; Kim, J.W.; Baek, S.; Lee, N. H.; Kim, S. J. Elucidation of phytochemicals and antioxidants properties of Sasa quelpaertensis. *Int. J. Food Prop.* **2021**, 24, 210-221.
44. Jiang, J.; Yu, X.; Fang, Y.; Zhang, Y., Li, N.; Wang, K. Chemical constituents of the roots of *Patrinia scabiosaefolia* and the cytotoxicity of patrineolignans A and B. *Chem.Nat. Comp.* **2017**, 53, 143-146.
45. Rasheed, M.U.; Thajuddin, N.; Ahamed, P.; Teklemariam, Z.; Jamil, K. Antimicrobial drug resistance in strains of Escherichia coli isolated from food sources. *Revis. do Instit. de Medic. Trop. de São Pau*. **2014**, 56, 341-346.
46. Abdallah, E.M.; Alhatlani, B.Y.; de Paula Menezes, R.; Martins, C.H.G. Back to Nature: Medicinal plants as promising sources for antibacterial drugs in the post-antibiotic era. *Plants* **2023**, 12, 1-27.
47. Veber, D.F.; Johnson, S.R.; Cheng, H.Y.; Smith, B.R., Ward, K.W.; Kopple, K.D. Molecular properties that influence the oral bioavailability of drug candidates. *J. Med. Chem.* **2002**, 45, 2615-2623.
48. Athar, M.; Sona, A.N.; Bekono, B.D.; Ntie-Kang, F. Fundamental physical and chemical concepts behind "drug-likeness" and "natural product-likeness". *Phys. Sci. Rev*. **2019**, 4, 1-18

49. Daina, A.; Michielin, O.; Zoete, V. SwissADME: a free web tool to evaluate pharmacokinetics, drug-likeness and medicinal chemistry friendliness of small molecules. *Sci. Rep*. **2017**, 7, 1-13.